J Electroceram (2011) 27:45–50
DOI 10.1007/s10832-011-9648-5

Raman and infrared spectroscopy of $Na_{0.5}Bi_{0.5}TiO_3$ - $BaTiO_3$ ceramics

Jan Suchanicz · Irena Jankowska-Sumara · Tatiana V. Kruzina

Received: 26 November 2010 / Accepted: 11 July 2011 / Published online: 20 July 2011
© The Author(s) 2011. This article is published with open access at Springerlink.com

Abstract Lead-free $Na_{0.5}Bi_{0.5}TiO_3$ -$BaTiO_3$ ceramics have been prepared in the whole range of concentrations and studied at room-temperature by means of X-ray, Raman scattering and infrared techniques. X-ray measurements revealed rhombohedral, rhombohedral-tetragonal boundaries and tetragonal modifacations depending on the contents of $BaTiO_3$. The distinct changes of the Raman and infrared spectra with increasing of $BaTiO_3$ content, which were correlated with X-ray results, were observed. The broad phonon spectra indicated the disorder in the A site of $Na_{0.5}Bi_{0.5}TiO_3$ -$BaTiO_3$ system.

Keywords NBT-BT ceramics · Ferroelectric · Raman and IR spectroscopy · Phase transformations

1 Introduction

Relaxor ferroelectrics have been widely studied due to their applications in a multi-layer capacitor and electromechanical transducer. Relaxor properties occur dominantly in lead-content compounds. However, the toxicity of lead-based components has caused the increasing interest in environment friendly compounds.

J. Suchanicz (✉) · I. Jankowska-Sumara
Institute of Physics, Pedagogical University,
ul Podchorazych 2,
30-084 Krakow, Poland
e-mail: sfsuchan@up.krakow.pl

T. V. Kruzina
Department of Physics, Dniepropetrovsk National University,
13 Nauchnyi per,
49-050 Dniepropetrovsk, Ukraine

$Na_{0.5}Bi_{0.5}TiO_3$ (NBT) and NBT-based ferroelectric materials are a promising environment friendly alternative to the more used toxic lead-content compounds [1–14].

NBT has two structural phase transitions from a paraelectric cubic phase to tetragonal one (520–540°C) and from tetragonal to a rhombohedral (ferroelectric) phase at about 260°C. There are some controversies over the number of phases existing in NBT and their electric order. The tetragonal modification is a ferroelastic [14] and probably polar phase [15, 16]. At about T_m=320°C a broad maximum of electric permittivity appears. This maximum does not correlate with any phase transition as well as the shift of T_m with the change of frequency, typical for relaxors, is not observed [11]. Nevertheless some relaxor-like behaviour can be induced after adding Ba ions to NBT [1–8].

$BaTiO_3$ (BT) is one of the mostly studied ferroelectric materials. There are three phase transitions: the first one from the cubic to tetragonal (ferroelectric) symmetry at about 120°C, the second one from the tetragonal to orthorhombic symmetry at about 5°C and the third one from the orhorhombic to rhombohedral symmetry at about −90°C.

There are a few papers concerning the Raman spectroscopy study of NBT [17–20] and NBT-based materials [21]. The results of the high-pressure Raman study of NBT [22] and 0.89NBT-0.11BT [23] have been reported recently. The measurements of polarized Raman spectra were performed for 0.94NBT-0.06BT single crystal [24]. The infrared study was performed for NBT [20, 24] and for the some compositions of solid solutions of NBT-PT and NBT-ST [25].

The present paper reports the results of the room-temperature Raman scattering and infrared studies of $Na_{0.5}Bi_{0.5}TiO_3$ -$BaTiO_3$ (NBT-BT) ceramics in the whole concentration range including the rhombohedral and rhombohedral-tetragonal boundaries and also tetragonal modifications.

2 Experimental procedure

The NBT-BT ceramics in the whole range of concentrations have been obtained by a three-stage conventional mixed oxide technique. The NBT and BT materials have been ground and then weighed in the proportion fulfiling the rule:

$$(1-x)Na_{0.5}Bi_{0.5}TiO_3 + xBaTiO_3 \rightarrow (Na_{0.5}Bi_{0.5})_{1-x}Ba_xTiO_3 (0 \leq x \leq 1)$$

Carefully mixed and then pressed the moulded piece of the obtained components have been sintered for the first time in the following conditions: 700–750°C for 1.5 h and 800–850°C for 2 h. The second stage was performed at 900–1000°C for 1 h, 1050–1200°C for 1 h and 1100–1300°C for 1 h. The conditions of the third sintering were as follows: 1100–1300°C for 1.5 h and 1160–1400°C for 2 h. The temperature of the second and the third sintering has been linearly increased within the above mentioned temperature range, with the increase of Ba^{2+} content. The obtained ceramics were cream-coloured, translucent, with the density greater than 95% of its theoretical values and they exhibited very good mechanical properties.

The X-ray diffraction measurements were performed by a modified DRON 1.5 diffractometer and controlled by a computer. The CuK_α radiation was filtered (λ=1.54056 Å). The powdered samples were investigated. Full-profile Rietveld refinements were carried out using a software package FullProf.

A scanning electron microscope (SEM), Hitachi S-4700 equipped with an energy dispersive X-ray spectrometer (EDS) with a Si(Li) X-ray detector, was used for the investigation of the microstructure of ceramics.

The Raman spectra of NBT-BT powders were obtained in a Bio-Rad FTS 6000 spectrometer with Nd-Yag laser system, where the 1064 nm line was used as an excitation line. The laser power was 200 mW. The spectra were collected with 4 cm^{-1} resolution.

The infrared spectra of NBT-BT powders were obtained using a Fourier transform spectrometer FTS 14.

For the Raman and IR spectra the samples were powdered and dispersed in KBr (1 mg of the sample per 100 mg of KBr). A standard method for the preparation of pressed pastilles was applied here.

Both Raman and IR spectra were analyzed using Jandel Scientific Peak fit 4.0 software. A second order polynomial was used to model the background while peaks were modeled as a sum of Lorenzian and Gaussian functions.

3 Results and discussion

Figure 1 gives the room-temperature XRD patterns of some NBT-BT ceramics. As can be seen, the obtained samples possess the single phase of perovskite-type structure. Their symmetry changes from rhombohedral over the rhombohedral-tetragonal phase boundary (for the composition about 0.94NBT-0.06BT) to tetragonal one for the higher contents of BT. The rhombohedral symmetry is characterized by a (003)/(021) peak splitting at around 40° and the single peak of (202) at around 46° (Fig. 1a). The coexistence of a rhombohedral-tetragonal phase is characterized by a (003)/(021) peak splitting at around 40° and (002)/(200) reflections at around 46° (Fig. 1b).With the increasing of BT content, the structure turned into the tetragonal symmetry with the (003) and (021) peaks combining into one peak and (002)/(200) reflections (Fig. 1c). Moreover, the progressive substitution of Na^+/Bi^{3+} by Ba^{2+} ions has provided to the increase in lattice constants (not shown here). This is in accordance with fact, that the

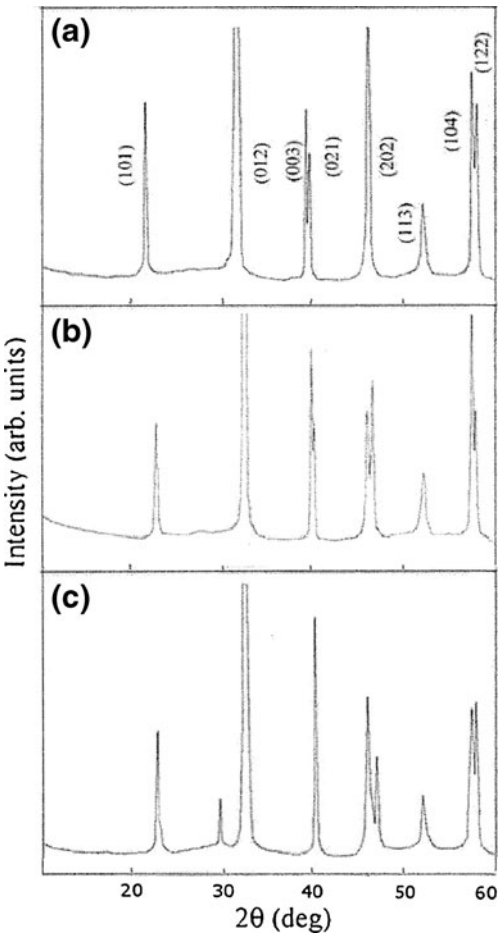

Fig. 1 XRD patterns of NBT (**a**), 0.94NBT-0.06BT (**b**) and 0.90NBT-0.10BT (**c**) ceramics

ionic radius of Ba^{2+} is much larger than the ionic radii of Na^{+} and Bi^{3+}, which leads to the increase in lattice parameters.

The investigation of the microstructure of the ceramics shows, that all samples have the dense microstructures and similar grain morphology with an average grain size ~(3–5)μm (the insert *a* in Fig. 2 shows an SEM graph of the fracture surface of 0.90NBT-0.10BT ceramic as a example). Almost no abnormal grain growth is observed. The Archimedes method gave the relative density of more than 95% of the theoretical values for all samples.

The atomic mass of barium (m_{Ba}=137.34) lies between the atomic mass of sodium (m_{Na}=22.99) and bismuth (m_{Bi}=208.98). Simultaneously the ionic radius of sodium (r_{Na}=1.02Å) and of bismuth (r_{Bi}=1.03Å) are comparable, but the ionic radius of barium (r_{Ba}=1.35Å) is fmuch greater. The admixture of barium ions to NBT, which causes the considerable distorstion of crystal structure and changes the force constants will influence the character of Raman and infrared spectra.

At the room temperature, NBT has the rhombohedral R3C phase, and the factor group analysis yields $4A_1$ (IR,R) +9 E (IR,R) optical modes which are represented in total 13 simultaneously IR and Raman active modes. On the other hand $BaTiO_3$ which is a well known classic ferroelectric, at room temperature is the ferroelectric with P4mm tetragonal structure. The cubic paraelectric phase Pm3m allows four optical modes $3F_{1u}+1F_{2u}$, that are not Raman active. Only $3F_{1u}$ modes are IR active (F_{2u} is so called silent mode). In the tetragonal phase of $BaTiO_3$ three A_1+E phonons arise from the three F_{1u} modes whereas one E+B_1 mode comes from the F_{2u} "silent mode". As a result we obtain 8 Raman active modes and seven IR active modes (7(IR+R)+1R).

The Raman spectra of (1-x)NBT-xBT ceramics are presented in Fig. 2. The spectra for NBT and for 0.9NBT-0.1BT are in general agreement with the other published for this materials Raman results [17–20, 23]. The Raman bands are relatively broad, which can be caused by the disorder in the sublattice A, the overlap of Raman modes and also by the ceramic form of the samples. When analysing Fig. 2 one can state that the evolution of Raman spectra with increasing of Ba^{2+} contents shows some interesting changes (see also Fig. 3):

1. the band at about 142 cm^{-1} decreases in intensity and displays a shift to lower frequencies (up to about 118 cm^{-1} for x=0.3),
2. the band at about 280 cm^{-1} splits into two modes at 260 and 310 cm^{-1}. The mode at 260 cm^{-1} decreases in intensity and finally disappears for 0.2NBT – 0.8BT,
3. the band around 400–650 cm^{-1} consists of three modes (at about: 490 cm^{-1}, 530 cm^{-1} and 585 cm^{-1}), the modes at 490 cm^{-1} and 585 cm^{-1} decrease in intensity leaving the mode at 530 cm^{-1} which the frequency decreases to about 520 cm^{-1} for 0.2NBT–0.8BT. Simultaneously a new line at about 620 cm^{-1} appears which the intensity

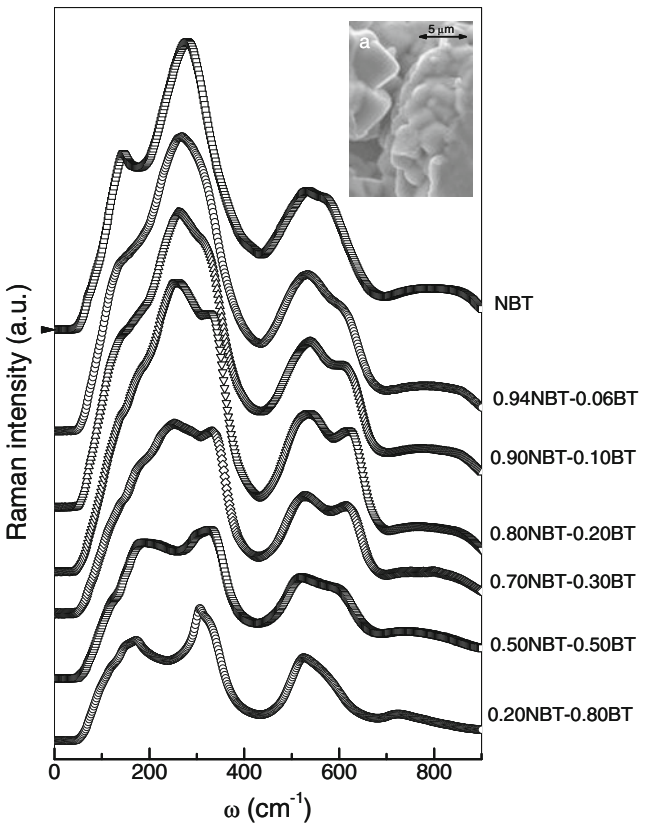

Fig. 2 Room temperature Raman spectra for (1-x)NBT-xBT ceramics. The insert *a* shows an SEM micrograph of a fracture surface of 0.90NBT-0.10BT ceramic

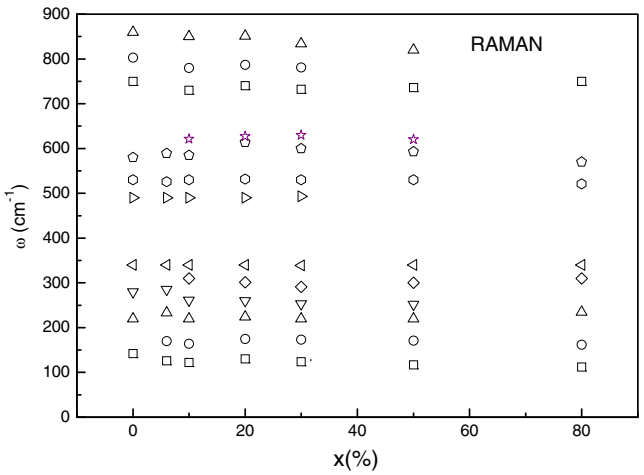

Fig. 3 Evolution of the Raman mode frequencies of (1-x)NBT-xBT ceramics

initially increases and shows maximum for 0.8NBT–0.2BT and than it decreases again,

4. the high frequency bands (for pure NBT at about: 740 cm^{-1}, 800 cm^{-1}, 860 cm^{-1}) overlaps into the single broad band (about 810 cm^{-1} for $BaTiO_3$ [25]).

The position and shape of 142 cm^{-1} band reveals changes when the content of admixture is changed, and probably that should be associated with the vibrations in sublattice A. This mode is probably associated with $A_1(TO_1)$ mode [26]. In present experiment the observed shift of this mode towards lower frequencies can be mainly caused by the increase in the mass of the cations of sublattice A, however the broadening of this band- with the increase of the degree of disorder in this sublattice. In the harmonic oscillator approximation, neglecting the changes of force constant, the mass and the frequency are connected according to the following dependence:

$$(f_{x=0}/f_{x=0.3})^2 \approx M_{x=0.3}/M_{x=0} \quad (1)$$

where $f_{x=0}/f_{x=0.3} \approx 1.10$. When analysing the mass effect the difficulty appears caused by the presence of three different ions (Na^+, Bi^{3+}, Ba^{2+}) in the sublattice A. There are two ways of solving this problem [21]. The first way is the usage of the so called virtual ion model, it means the ion with the average properties of cations in sublattice A. This model is useful when the little difference of masses and force constants takes place, which does not occur for NBT. The Bi^{3+} mass is considerably greater than Na^+ mass, and the force constants are different because the bondings Na-O and Bi-O are different. The shift of band 142 cm^{-1} calculated on the base of this model is considerably less than this one observed in the experiment. The second way is the usage of the multimode model of behaviour, in which the material is treated as the complex of different areas, which are rich of the first or of the second component

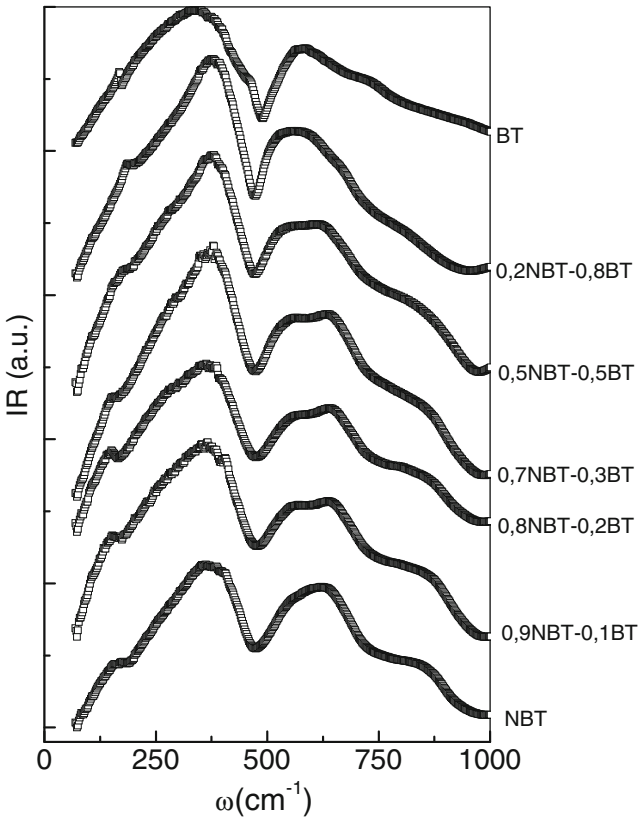

Fig. 5 Room temperature infrared absorption spectra for (1-x)NBT-xBT ceramics

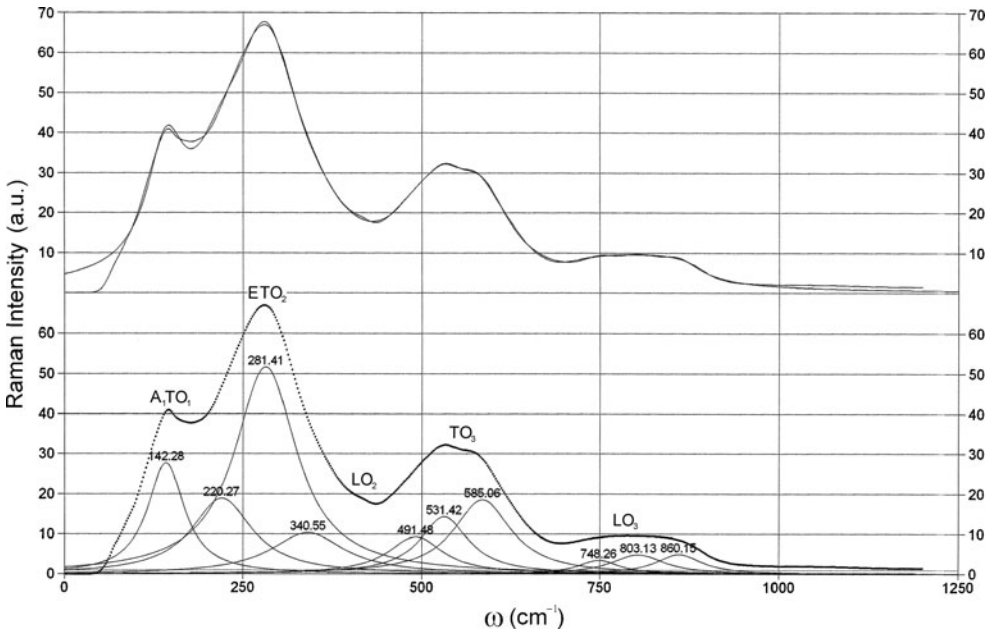

Fig. 4 Fitting of the Raman spectra of NBT ceramic to the Lorentzian function

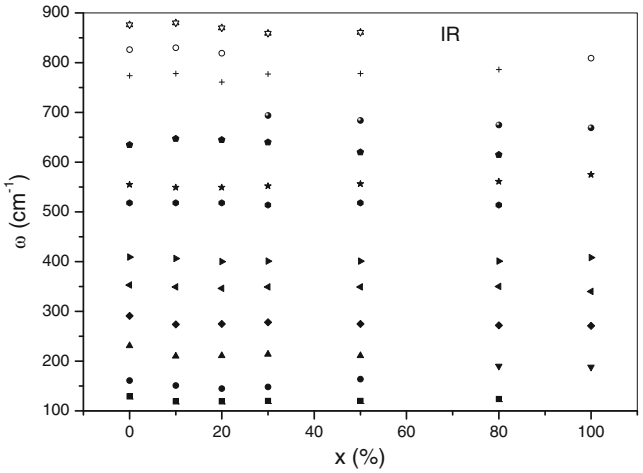

Fig. 6 Evolution of the infrared absorption mode frequencies of (1-x) NBT-xBT ceramics

respectively. In NBT it should cause the splitting of Na-O and Bi-O bands, but in NBT-BT − Na-O, Bi-O and Ba-O bands. It should lead to arise at least one additional line in the Raman spectra, which was confirmed by the experimental results (Fig. 2). Simultaneously the experimental value $(f_{x=0}/f_{x=0.3})^2 \approx 1.10$ agrees with $0.7\ m_{(Na\ 0.5\ Bi0.5)} + 0.3m_{Ba}/m_{(Na0.5Bi0.5)} \approx 1.06$.

The band at ~280 cm^{-1} – $E(TO_2)$ - can be observed in many perovskite materials. The first changes are accompanied by the arising of the additional line (~310 cm^{-1}) – LO_2 - in the high frequency part of this band and they can already be seen for the compound 0.94NBT-0.06BT. This compound is characterized by the morphotropic phase boundary between rhombohedral and tetragonal phases. The additional line is already considerably seen for the compound 0.9NBT-0.1BT, which exhibits the tetragonal symmetry. These facts give the evidence, that the arising of the additional line (~310 cm^{-1}) is connected with the appearance of tetragonal structure.

According to the results of investigations of another perovskite materials, the TO_3 bands at 530 cm^{-1} and 585 cm^{-1} should be sensitive to the changes of structure. The evolution of these bands with the change of the contents of BT is evidenced in Fig. 2. Particularly it concerns the band 585 cm^{-1}, which behaviour is similar to this additional band 310 cm^{-1} connected with the change of structure from rhombohedral to tetragonal. The high-freguency Raman bands, in the case of oxides, are usually caused by the vibrations resulting from the shift of oxygen [21]. For this reason one can expect, that they do not depend on the mass of cation. But the cation can influence the frequency position of these bands, for example through the force constant. The evolution of 530 cm^{-1} and 585 cm^{-1} bands can be caused by the increasing the average ion radius of cations in sublattice A with the increase of BT content.

In general the frequencies of particular modes do not vary much with composition (Fig. 3). The sample fitting of the Raman spectrum to the Lorentzian function is presented in Fig. 4.

The IR spectra for (1-x)NBT–xBT are generally similar to those observed in the Raman investigations (Figs. 5 and 2 for comparison). The main difference which can be observed in this spectra is the shift of the respective modes to the higher frequencies. This difference can be explained taking into consideration the random grain orientations in the ceramics. Because of it the directions of the phonon

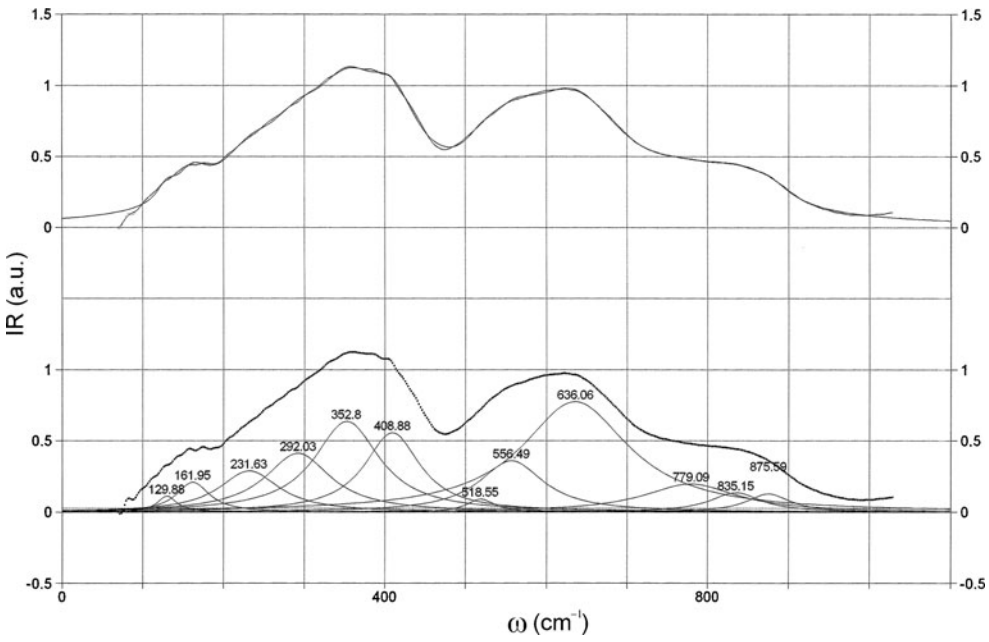

Fig. 7 Fitting of the infrared absorption spectra of NBT ceramic to the Lorentzian function

wave vectors are randomly distributed from one grain to another with respect to the crystallographic axes. As a result the Raman and also IR lines in ceramics resulting from the mode mixing and long range electrostatic force effects are relatively broader than that found in single crystals. The phonon frequencies also shift remarkably to higher/lower values depending upon the finite size of the powder grains and due to depelarization fields [27]. This can be the reason for the shifting of frequencies between the Raman and IR measurements. The IR spectra for NBT (Fig. 5) are similar to those described by Petzelt et al. [20] and Lee et al. [25]. The evolution of the mode frequencies for the different compositions of NBT–BT ceramics is presented in Fig. 6. As for the Raman results, the frequencies of particular modes do not vary much with composition. The fitting of the IR spectrum of NBT to the Lorentzian function is presented in Fig. 7.

According to the literature data [28], $BaTiO_3$ Raman spectrum contains the sharp mode $A_1(TO_1)$ at about 170 cm^{-1} which interferes with broad $A_1(TO_2)$ mode about 270 cm^{-1} and results as a resonance effect at 174 cm^{-1}. This effect is very slightly seen in our Raman spectra but very clearly seen in the IR measurements at about 165 cm^{-1} (see Fig. 5). This coupling weakens with changing the composition in the direction of NBT and the new line at 124 cm^{-1} appears for 0.2NBT −0.8BT in the IR spectra.

4 Summary

Lead-free NBT-BT solid solutions were prepared in the whole range of concentrations via the conventional mixed oxide route. The room-temperature X-ray, Raman scattering and infrared investigations of those materials were performed. It was shown from the X-ray measurements, that the substitution of Na^+/Bi^{3+} by Ba^{2+} ions caused the modification changes from rhombohedral over rhombohedral-tetragonal to tetragonal boundaries and the increase in lattice parameters. The changes of Raman and infrared spectra with increasing of BT contents, were observed and discussed in details in accordance with the structure changes.

Open Access This article is distributed under the terms of the Creative Commons Attribution Noncommercial License which permits any noncommercial use, distribution, and reproduction in any medium, provided the original author(s) and source are credited.

References

1. Y.M. Chiang, G.W. Farrey, A.N. Soukhojak, Appl. Phys. Lett. **73**, 3683 (1998)
2. S.A. Sheets, A.N. Soukhojak, N. Ohashi, Y.M. Chiang, J. Appl. Phys. **90**, 5287 (2001)
3. J. Suchanicz, J.P. Mercurio, K. Konieczny, Ferroelectrics **268**, 357 (2002)
4. J. Suchanicz, J. Kusz, H. Böhm, Mat. Sci. Eng. **B97**, 154 (2003)
5. Bao-Jin Chu, Guo-Rong Li, Xiang-Ping Jiang, Da-Ren Chen, J. Inorg.Mat. **15**, 815 (2000). in Chinesse
6. Bao-Jin Chu, Guo-Rong Li, Qing-Rui Yin, Wang-Zhong Zhang, Chen, Acta Phys. Sinica **50**, 2012 (2001). in Chinesse
7. J. Suchanicz, J. Kusz, H. Böhm, H. Duda, J.P. Mercurio, K. Konieczny, J. Eur. Cer. Soc. **23**, 1559 (2003)
8. J. Suchanicz, J. Kusz, H. Böhm, G. Stopa, J. Mater. Sci. **42**, 7827 (2007)
9. J. Kusz, J. Suchanicz, H. Böhm, J. Warczewski, Phase Transitions **70**, 223 (1999)
10. T. Takenaka, K. Maruyama, K. Sakata, Jpn.J.Appl.Phys **30**, 2236 (1991)
11. J.Suchanicz, I.P.Mercurio, P.Marchet and T.V.Kruzina, Phys.Stat. Sol., **(b)225**, 459 (2001)
12. J. Suchanicz, Mat.Sci.Eng **B55**, 114 (1998)
13. J. Suchanicz, Ferroelectrics **209**, 561 (1998)
14. S.E. Park, S.J. Chung, J. Am. Cer. Soc. **79**, 1290 (1996)
15. G.O. Jones, P.A. Thomas, Acta Crystallogr. **B56**, 426 (2000)
16. G.O. Jones, P.A. Thomas, Acta Crystallogr. **B58**, 168 (2002)
17. I.G. Siny, T.A. Smirnova, T.V. Kruzina, Ferroelectrics **124**, 207 (1991)
18. M. Zhang, I.F. Scott, I.A. Zvirgds, Ferroelectrics **6**, 147 (1986)
19. I.G. Siny, E. Husson, I.M. Beny, S.G. Lushnikov, E.A. Rogacheva, P.P. Syrnikov, Physica **B293**, 382 (2001)
20. J. Petzelt, S. Kamba, J. Fabry, D. Noujni, V. Porokhonsky, A. Pashkin, I. Franke, K. Roleder, J. Suchanicz, R. Klein, G.E. Kugel, J.Phys.:Condens.Matter **16**, 2719 (2004)
21. J. Kreisel, A.M. Glazer, G.O. Jones, P.A. Thomas, P.A. Abello, G. Lucazeau, J. Phys. Condens. Matter **12**, 3267 (2000)
22. J. Kreisel, A.M. Glazer, P. Bouvier, G. Lucazeau, Phys. Rev. **B63**, 174106 (2001)
23. S. Trujillo, J. Kreisel, Q. Jiang, J.H. Smith, P.A. Thomas, P. Bouvier, F. Weiss, J.Phys.:Condens.Matter **17**, 6587 (2005)
24. I. Gregora, P. Ondrejkovic, E. Simon, M. Berta, M. Savinov, J. Hlinka, H. Luo, Q. Zhang, Ferrroelectrics **404**, 220 (2010)
25. J.K. Lee, K.S. Houg, C.K. Kim, S.E. Park, J. Appl. Phys. **91**, 4538 (2002)
26. E. Buixaderas, S. Kamba, J. Petzelt, J. Drahokoupil, F. Laufek, M. Kosec, Appl. Phys. Lett. **91**, 112909 (2007)
27. J.T. Luxon, D.J. Montgomery, R. Summit, J. Appl. Phys. **41**, 2303 (1970)
28. P.S. Dobal, A. Dixit, R.S. Katiyar, Z. Yu, R. Guo, A.S. Bhalla, J. Appl. Phys. **89**, 8085 (2001)